On the viability of small endohedral hydrocarbon cage complexes: X@C 4H4, X@C8H8, X@C8H 14, X@C10H16, X@C12H12, and X@C16H16

ARTICLE *in* JOURNAL OF THE AMERICAN CHEMICAL SOCIETY · OCTOBER 2003

Impact Factor: 12.11 · DOI: 10.1021/ja0345470 · Source: PubMed

5 AUTHORS, INCLUDING:

Henry Lee Woodcock
University of South Florida
55 PUBLICATIONS **4,769** CITATIONS

SEE PROFILE

Zhongfang Chen
University of Puerto Rico at Rio Piedras
220 PUBLICATIONS **7,983** CITATIONS

SEE PROFILE

J|A|C|S
ARTICLES
Published on Web 08/22/2003

On the Viability of Small Endohedral Hydrocarbon Cage Complexes: X@C_4H_4, X@C_8H_8, X@C_8H_{14}, X@$C_{10}H_{16}$, X@$C_{12}H_{12}$, and X@$C_{16}H_{16}$

Damian Moran,[†,‡] H. Lee Woodcock,[†] Zhongfang Chen,[†,‡] Henry F. Schaefer III,[†] and Paul v. R. Schleyer*[,†,‡]

Contribution from the Center for Computational Quantum Chemistry, University of Georgia, Athens, Georgia 30602, and Institut für Organische Chemie der Universität Erlangen-Nürnberg, Henkestrasse 42, D-91054 Erlangen, Germany

Received February 7, 2003; E-mail: schleyer@chem.uga.edu

Abstract: Small hydrocarbon complexes (X@cage) incorporating cage-centered endohedral atoms and ions (X = H^+, H, He, Ne, Ar, $Li^{0,+}$, $Be^{0,+,2+}$, $Na^{0,+}$, $Mg^{0,+,2+}$) have been studied at the B3LYP/6-31G(d) hybrid HF/DFT level of theory. No tetrahedrane (C_4H_4, T_d) endohedral complexes are minima, not even with the very small hydrogen atom or beryllium dication. Cubane (C_8H_8, O_h) and bicyclo[2.2.2]octane (C_8H_{14}, D_{3h}) minima are limited to encapsulating species smaller than Ne and Na^+. Despite its intermediate size, adamantane ($C_{10}H_{16}$, T_d) can enclose a wide variety of endohedral atoms and ions including H, He, Ne, $Li^{0,+}$, $Be^{0,+,2+}$, $Na^{0,+}$, and Mg^{2+}. In contrast, the truncated tetrahedrane ($C_{12}H_{12}$, T_d) encapsulates fewer species, while the D_{4d} symmetric $C_{16}H_{16}$ hydrocarbon cage (see Table of Contents graphic) encapsulates all but the larger Be, Mg, and Mg^+ species. The host cages have more compact geometries when metal atoms, rather than cations, are inside. This is due to electron donation from the endohedral metals into C−C bonding and C−H antibonding cage molecular orbitals. The relative stabilities of endohedral minima are evaluated by comparing their energies (E_{endo}) to the sum of their isolated components ($E_{inc} = E_{endo} - E_{cage} - E_x$) and to their exohedral isomer energies ($E_{isom} = E_{endo} - E_{exo}$). Although exohedral binding is preferred to endohedral encapsulation without exception (i.e., E_{isom} is always exothermic), Be^{2+}@$C_{10}H_{16}$ (T_d; −235.5 kcal/mol), Li^+@$C_{12}H_{12}$ (T_d; 50.2 kcal/mol), Be^{2+}@$C_{12}H_{12}$ (T_d; −181.2 kcal/mol), Mg^{2+}@$C_{12}H_{12}$ (T_d; −45.0 kcal/mol), Li^+@$C_{16}H_{16}$ (D_{4d}; 13.3 kcal/mol), Be^+@$C_{16}H_{16}$ (C_{4v}; 31.8 kcal/mol), Be^{2+}@$C_{16}H_{16}$ (D_{4d}; −239.2 kcal/mol), and Mg^{2+}@$C_{16}H_{16}$ (D_{4d}; −37.7 kcal/mol) are relatively stable as compared to experimentally known He@$C_{20}H_{20}$ (I_h), which has an E_{inc} = 37.9 kcal/mol and E_{isom} = −35.4 kcal/mol. Overall, endohedral cage complexes with low parent cage strain energies, large cage internal cavity volumes, and a small, highly charged guest species are the most viable synthetic targets.

Introduction

Cage molecules[1−7] with atoms and ions inside are not only significant theoretically[8−17] but also may have intriguing practical uses.[18−21] Endohedral cage complexes[22] (X@cage) have potential applications as magnetic resonance imaging contrast agents,[23] semiconductors, and ferromagnets.[24] Saunders and coworkers[25] have used endohedral helium atoms and NMR to

† University of Georgia.
‡ Institut für Organische Chemie der Universität Erlangen-Nürnberg.

(1) Wrackmeyer, B.; Schanz, H. J.; Hofmann, M.; Schleyer, P. v. R. *Angew. Chem., Int. Ed.* **1998**, *37*, 1245.
(2) McEwen, A.; Schleyer, P. v. R. *J. Am. Chem. Soc.* **1986**, *108*, 3951.
(3) Schleyer, P. v. R. In *Cage Hydrocarbons*; Olah, G. A., Ed.; Wiley: New York, 1990; pp 1−38.
(4) Alder, R. W.; Harvey, J. N.; Schleyer, P. v. R.; Moran, D. *Org. Lett.* **2001**, *3*, 3233.
(5) Prinzbach, H.; Weiler, A.; Landenberger, P.; Wahl, F.; Worth, J.; Scott, L. T.; Gelmont, M.; Olevano, D.; Issendorff, B. v. *Nature* **2000**, *407*, 60.
(6) Kroto, H. W.; Heath, J. R.; O'Brien, S. C.; Curl, R. F.; Smalley, R. E. *Nature* **1985**, *318*, 162.
(7) Kroto, H. W.; Allaf, A. W.; Balm, S. P. *Chem. Rev.* **1991**, *91*, 1213.
(8) Charkin, O. P.; Klimenko, N. M.; Moran, D.; Mebel, A. M.; Schleyer, P. v. R. *Russ. J. Inorg. Chem.* **2001**, *46*, 110.
(9) Charkin, O. P.; Klimenko, N. M.; Moran, D.; Mebel, A. M.; Charkin, D. O.; Schleyer, P. v. R. *Inorg. Chem.* **2001**, *40*, 6913.
(10) Charkin, O. P.; Klimenko, N. M.; Moran, D.; Mebel, A.; Charkin, D. O.; Schleyer, P. v. R. *J. Phys. Chem. A* **2002**, *106*, 11594.
(11) Moran, D.; Stahl, F.; Jemmis, E. D.; Schaefer, H. F., III; Schleyer, P. v. R. *J. Phys. Chem. A* **2002**, *106*, 5144.
(12) Cioslowski, J. *Electrostatic Structure Calculations on Fullerenes and Their Derivatives*; Oxford University Press: New York, 1995.
(13) Billups, W. E., Ciufolini, M. A., Eds. *Buckminsterfullerenes*; VCH Publishers: New York, 1993.
(14) Schleyer, P. v. R.; Najafian, K.; Mebel, A. *Inorg. Chem.* **1998**, *37*, 6765.
(15) Jemmis, E. D.; Balakrishnarajan, M. M. *J. Am. Chem. Soc.* **2000**, *122*, 7392.
(16) Jemmis, E. D.; Jayasree, E. G. *Collect. Czech. Chem. Commun.* **2002**, *67*, 965.
(17) Chen, Z.; Jiao, H.; Moran, D.; Hirsch, A.; Thiel, W.; Schleyer, P. v. R. *J. Phys. Chem. A* **2003**, *107*, 2075.
(18) Weiske, T.; Schwarz, H.; Hirsch, A.; Grosser, T. *Chem. Phys. Lett.* **1992**, *199*, 640.
(19) Weiske, T.; Bohme, D. K.; Hrusak, J.; Kratschmer, W.; Schwarz, H. *Angew. Chem., Int. Ed. Engl.* **1991**, *30*, 884.
(20) Rose, H. R.; Dance, I. G.; Fisher, K. J.; Smith, D. R.; Willett, G. D.; Wilson, M. A. *Org. Mass Spectrom.* **1994**, *29*, 470.
(21) Saunders, M.; Jimenez-Vazquez, H. A.; Cross, R. J.; Mroczkowski, S.; Gross, M. L.; Giblin, D. E.; Poreda, R. J. *J. Am. Chem. Soc.* **1994**, *116*, 2193.
(22) Species listed to the left of the "@" are endohedrally encapsulated.
(23) Shinohara, H. *Rep. Prog. Phys.* **2000**, *63*, 843.
(24) Irle, S.; Rubin, Y.; Morokuma, K. *J. Phys. Chem. A* **2002**, *106*, 680.
(25) Saunders, M.; Cross, R. J.; Jimenez-Vazquez, H. A.; Shimshi, R.; Khong, A. *Science* **1996**, *271*, 1693.

10.1021/ja0345470 CCC: $25.00

probe the internal electronic and magnetic cage environment of fullerenes and provide experimental conformation of computational results such as nucleus independent chemical shift[26−28] predictions of cluster aromaticity.[29−32]

Fullerene endohedral complexes, incorporating 60 or more cage atoms (e.g., $ErSc_3N@C_{80}$),[33] have been extensively prepared in covaporization experiments,[33−35] using collisional insertion within a mass spectrometer,[18−20] by forced incorporation under high pressure (3000 atm, 650 °C),[21] and using molecular bombardment experiments.[36] The smallest endohedral hydrocarbon cage complex reported to date is $He@C_{20}H_{20}$, which was created by Cross, Saunders, and Prinzbach[37] when they blasted dodecahedrane[38,39] with a helium molecular beam.[36] Prior computations on $He@C_{20}H_{20}$ predicted that the endohedral dodecahedrane derivative was 38 kcal/mol higher in energy than its isolated components.[11] Furthermore, Mascal[40] predicted that the barrier to He ingression via a $C_{20}H_{20}$ face (i.e., along C_5 axis) is >300 kcal/mol, making the achievement of Cross, Saunders, and Prinzbach[37] all the more remarkable.

Mascal[40] also predicted large (100−200 kcal/mol) endothermic $C_{20}H_{20}$ facial entrance barriers for Li^+, Be^+, and Mg^{2+}. H^+ and Be^{2+} dodecahedrane entrance along a C_5 axis, however, was exothermic by ∼150 kcal/mol, and their concave potential energy profiles (energy vs distance from cage center) show points of inflection at cage face centers. Mascal's[40] Be^{2+} potential profile was in excellent agreement with our[11] previous computations showing that beryllium dication was a minimum with exothermically (>200 kcal/mol) bound internal and external cage faces (i.e., the potential energy profile is a double well potential with minima corresponding to exo- and endohedral facial binding). We[11] previously computed the relative energies of H, He, Ne, Ar, Li, Li^+, Be, Be^+, Na, Na^+, Mg, Mg^+, and Mg^{2+} dodecahedrane endohedral complexes and found that only $Li^+@C_{20}H_{20}$ (I_h), $Be^+@C_{20}H_{20}$ (C_{5v}), $Be^{2+}@C_{20}H_{20}$ (C_{5v}), and $Mg^{2+}@C_{20}H_{20}$ (I_h) had exothermic inclusion energies relative to their isolated components ($E_{inc} = E_{endo} - E_{cage} - E_x$). Although all of the endohedral dodecahedrane complexes were higher (>10 kcal/mol) in energy than their corresponding exohedral isomers, that is, external cage binding was favored, the Li^+, Be^{2+}, and Mg^{2+} relative energy differences were less than that of the known He complex, and they may also be synthesized in beam implantation experiments.

In light of the recent $He@C_{20}H_{20}$ preparative success,[37] we have now extended our previous DFT studies of endohedral dodecahedrane, borane, alane, and gallane complexes[8−11,14,15,17] to the smaller hydrocarbon cage systems T_d tetrahedrane (C_4H_4, **1**),[41−43] O_h cubane (C_8H_8, **2**),[44] D_{3d} bicyclo[2.2.2]octane (C_8H_{14}, **3**),[45,46] T_d adamantane ($C_{10}H_{16}$, **4**),[47−49] T_d truncated tetrahedrane ($C_{12}H_{12}$, **5**),[50,51] D_{3d} diamantane ($C_{14}H_{20}$, **6**),[52,53] and the D_{4d} symmetric 4,4-bitruncated tetragonal trapezohedron hydrocarbon isomer ($C_{16}H_{16}$, **7**) shown in Figure 1. We are seeking answers to a number of questions. Both H and Ar species are minima at the center of dodecahedrane,[11] but what are the analogous limits of encapsulation for the cages shown in Figure 1? Dodecahedrane is more compact when encapsulating a metal as compared to the corresponding cation/dication, due to donation of electron density from encapsulated metal atoms into the C−C bonding and C−H antibonding endohedral complex HOMO.[11] Do other endohedral hydrocarbon cage complexes respond to metal encapsulation similarly? $M@C_{20}H_{20}$ (M = Li, Na, Be, Mg) species possess lower first ionization potentials than the Cs atom (3.9 eV); that is, they are superalkalis.[11] Are the ionization potentials of metals encapsulated by the cages shown in Figure 1 also dramatically reduced? Relative to their isolated components, $X@C_{20}H_{20}$ (X = Li^+, Be^{2+}, Mg^{2+}) complexes have endohedral inclusion energies comparable to that of $He@C_{20}H_{20}$ and are promising synthetic targets. Are endohedral X@cage complexes incorporating hosts smaller than dodecahedrane also likely to be experimentally observable; that is, are they viable? Our results, which extend earlier theoretical predictions, highlight the size dependence of endohedral complex stability and reveal the dramatic effects of encapsulation on the ionization potentials of the enclosed atoms.

Computational Details

Endohedral complexes were optimized at the B3LYP/6-31G(d) hybrid HF/DFT level of theory; vibrational frequency analyses (at the same level) characterized the optimized structures as minima or higher and provided zero-point energies which are included throughout (ZPE; unscaled).[54−56] The B3LYP functional was chosen because the inclusion of electron correlation was important for accurate geometry prediction. For example, $Mg@C_{10}H_{16}$ (T_d) and $Mg^+@C_{10}H_{16}$ (T_d) were minima at

(26) Schleyer, P. v. R.; Maerker, C.; Dransfeld, A.; Jiao, H. J.; Hommes, N. J. r. V. E. *J. Am. Chem. Soc.* **1996**, *118*, 6317.
(27) Schleyer, P. v. R.; Jiao, H.; Hommes, N. J. R. v. E.; Malkin, V. G.; Malkina, O. L. *J. Am. Chem. Soc.* **1997**, *119*, 12669.
(28) Schleyer, P. v. R.; Manoharan, M.; Wang, Z.-X.; Kiran, B.; Jiao, H.; Puchta, R.; Hommes, N. J. R. v. E. *Org. Lett.* **2001**, *3*, 2465.
(29) Bühl, M.; Thiel, W.; Jiao, H. J.; Schleyer, P. v. R.; Saunders, M.; Anet, F. A. L. *J. Am. Chem. Soc.* **1994**, *116*, 6005.
(30) Bühl, M.; Patchkovskii, S.; Thiel, W. *Chem. Phys. Lett.* **1997**, *275*, 14.
(31) Bühl, M. *Chem.-Eur. J.* **1998**, *4*, 734.
(32) Hirsch, A.; Chen, Z.; Jiao, H. *Angew. Chem., Int. Ed.* **2001**, *40*, 2834.
(33) Stevenson, S.; Rice, G.; Class, T.; Harich, K.; Cromer, F.; Jordan, M. R.; Craft, J.; Hadju, E.; Bible, R.; Olmstead, M. M.; Maitra, K.; Fisher, A. J.; Balch, A. L.; Dorn, H. C. *Nature* **1999**, *401*, 55.
(34) Krätschmer, W.; Fostiropoulos, K.; Lamb, L. D.; Huffman, D. R. *Nature* **1990**, *347*, 354.
(35) Heath, J. R.; O'Brien, S. C.; Zhang, Q.; Liu, Y.; Curl, R. F.; Kroto, H. W.; Smalley, R. E. *J. Am. Chem. Soc.* **1985**, *107*, 7779.
(36) Shimshi, R.; Cross, R. J.; Saunders, M. *J. Am. Chem. Soc.* **1997**, *119*, 1163.
(37) Cross, R. J.; Saunders, M.; Prinzbach, H. *Org. Lett.* **1999**, *1*, 1479.
(38) Ternansky, R. J.; Balogh, D. W.; Paquette, L. A. *J. Am. Chem. Soc.* **1982**, *104*, 4503.
(39) Fessner, W. D.; Murty, B.; Worth, J.; Hunkler, D.; Fritz, H.; Prinzbach, H.; Roth, W. D.; Schleyer, P. v. R.; McEwen, A. B.; Maier, W. F. *Angew. Chem., Int. Ed. Engl.* **1987**, *26*, 452.
(40) Mascal, M. *J. Org. Chem.* **2002**, *67*, 8644.
(41) Notario, R.; Castano, O.; Andres, J. L.; Elguero, J.; Maier, G.; Hermann, C. *Chem.-Eur. J.* **2001**, *7*, 342.
(42) Balci, M.; McKee, M. L.; Schleyer, P. v. R. *J. Phys. Chem. A* **2000**, *104*, 1246.
(43) Balci, M.; McKee, M. L.; Schleyer, P. v. R. *J. Phys. Chem. A* **2000**, *104*, 6338.
(44) Eaton, P. E.; Cole, T. W., Jr. *J. Am. Chem. Soc.* **1964**, *86*, 3157.
(45) Schleyer, P. v. R.; Blanchard, K. R.; Woody, C. D. *J. Am. Chem. Soc.* **1963**, *85*, 1358.
(46) McAllister, T.; Dolesek, Z.; Lossing, F. P.; Gleiter, R.; Schleyer, P. v. R. *J. Am. Chem. Soc.* **1967**, *89*, 5982.
(47) Fort, R. C.; Schleyer, P. v. R. *Chem. Rev.* **1964**, *64*, 277.
(48) Schleyer, P. v. R. *J. Am. Chem. Soc.* **1957**, *79*, 3292.
(49) Schleyer, P. v. R.; Donaldson, M. M.; Nicholas, R. D.; Cupas, C. A. *Org. Synth.* **1962**, *42*, 8.
(50) Bettinger, H. F.; Pak, C. H.; Xie, Y. M.; Schleyer, P. v. R.; Schaefer, H. F. *J. Chem. Soc., Perkin Trans. II* **1999**, 2377.
(51) Disch, R. L.; Schulman, J. M. *J. Am. Chem. Soc.* **1990**, *112*, 3377.
(52) Grubmüller, P.; Maier, W. F.; Schleyer, P. v. R.; McKee, M. A.; Rooney, J. J. *Chem. Ber.* **1980**, *113*, 1989.
(53) Osawa, E.; Furusaki, A.; Hashiba, N.; Matsumoto, T.; Singh, V.; Tahara, Y.; Wiskott, E.; Farcasiu, M.; Iizuka, T.; Tanaka, N.; Kan, T.; Schleyer, P. v. R. *J. Org. Chem.* **1980**, *45*, 2985.
(54) Hehre, W. J.; Radom, L.; Pople, J. A.; Schleyer, P. v. R. *Ab Initio Molecular Orbital Theory*; John Wiley & Sons: New York, 1986.
(55) Schleyer, P. v. R.; Allinger, N. L.; Clark, T.; Gasteiger, J.; Kollman, P. A.; Schaefer, H. F., III; Schreiner, P. R. *The Encyclopedia of Computational Chemistry*; John Wiley & Sons. Ltd.: Chichester, 1998.
(56) Foresman, J. B.; Frisch, M. J. *Exploring Chemistry with Electronic Structure Methods*, 2nd ed.; Gaussian, Inc.: Pittsburgh, PA, 1996.

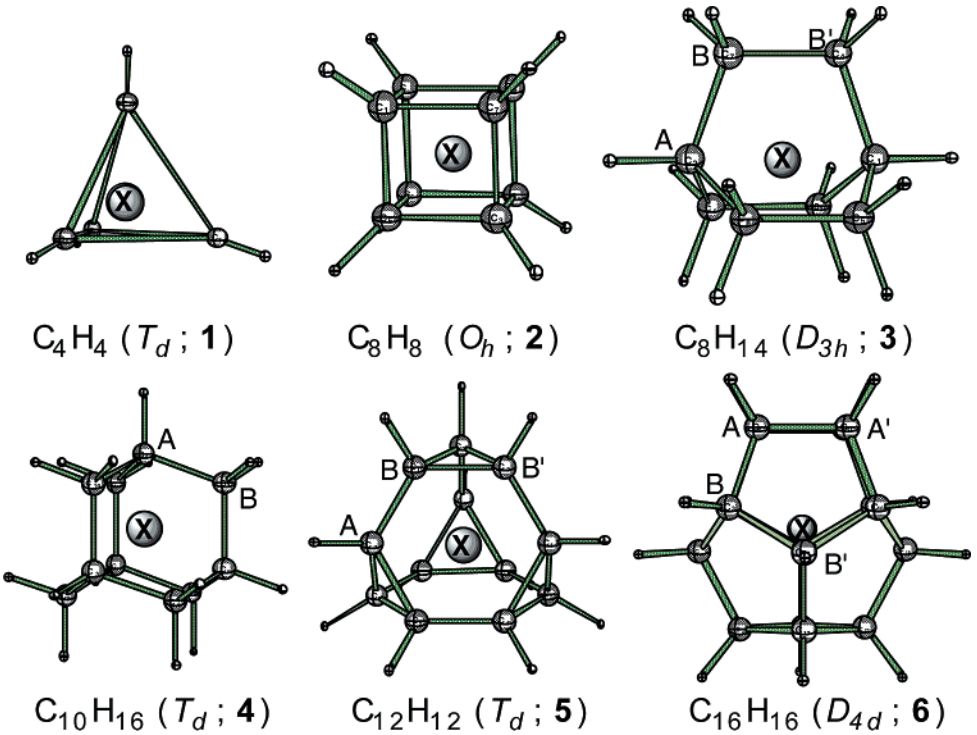

Figure 1. Hydrocarbon cages with endohedrally encapsulated "X" species.

HF/6-31G(d); however, they had five (doubly degenerate 789*i* cm^{-1} and triply degenerate 461*i* cm^{-1}) and three (triply degenerate 2222*i* cm^{-1}) imaginary frequencies, respectively, at B3LYP/6-31G(d). DFT methods were used in preference to correlated ab initio methods such as MP2 because of the large basis set superposition errors[11,57,58] and lengthy execution times associated with the latter. Furthermore, consistent with our[11] previous $He@C_{20}H_{20}$ and $Ne@C_{20}H_{20}$ results, agreement between, for example, $Be^{2+}@C_8H_8$ B3LYP/6-31G(d) (E_{inc} = −69.8 kcal/mol; E_{bind} = −222.0 kcal/mol; and E_{isom} = −152.2 kcal/mol) and MP2/6-31G(d) (E_{inc} = −68.7 kcal/mol; E_{bind} = −216.7 kcal/mol; and E_{isom} = −148.5 kcal/mol) relative energies (see below for energy term definitions) was <5 kcal/mol. The 6-31G(d) basis set was used throughout because B3LYP/6-31G(d) + ZPE and B3LYP/6-311+G(d,p) + ZPE relative energies are generally in good agreement (<1 kcal/mol). For example, $H@C_{20}H_{20}$ and $He@C_{20}H_{20}$ inclusion energies (*vide infra*) are (B3LYP/6-31G(d) + ZPE) 36.3 and 38.0 kcal/mol,[17] respectively, and (B3LYP/6-311+G(d,p) + ZPE) 35.8 and 37.9 kcal/mol,[11] respectively. Endohedral complexes where the cage was possibly overly "stretched" were checked for wave function instabilities, for example, $Be@C_{10}H_{16}$ (T_d); however, none were found.

The inclusion energies, E_{inc} (kcal/mol), of endohedral complex minima were evaluated by comparing the energy of X@cage (E_{endo}) to the sum of the energies of the isolated components, E_{cage} and E_x. For comparison, their corresponding exohedral binding energies (E_{bind}, kcal/mol), which is the energy difference between the most stable exohedral structures (E_{exo}) and the sum of the isolated component energies, were also computed. We designated the energy difference between the most stable exohedral structures and their endohedral isomers as the "isomerization energy", E_{isom} (kcal/mol). The values of E_{inc}, E_{bind}, and E_{isom} are represented graphically in Figure 2. All energies were corrected using unscaled zero-point energies (ZPE).

The optimized endohedral complexes were used to calculate adiabatic ionization potentials and to obtain NBO[59] natural charges. Cage and

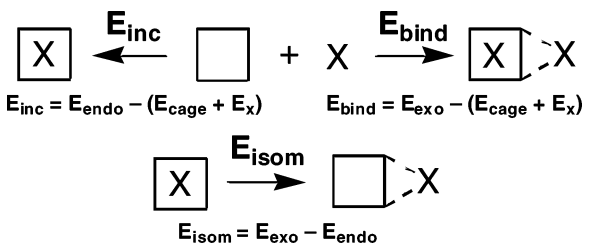

Figure 2. Graphical summary of inclusion, binding, and isomerization energies (kcal/mol).

ring cyclic electron delocalization was assessed using NICS at the GIAO/B3LYP/6-31G(d)//B3LYP/6-31G(d) level.[26−28] All calculations were performed using Gaussian 98.[60] Absolute energies, ZPE, optimized endohedral bond lengths, and unscaled lowest (real or imaginary) vibrational frequencies are summarized in the Supporting Information.

Results and Discussion

$X@C_4H_4$ (T_d). As could be expected, all endohedral complexes of tetrahedrane ($X@C_4H_4$) are B3LYP/6-31G(d) higher order stationary points (NImag ≥ 2), with both the small internal volume (0.143 $Å^3$; Table 1) of the cage and the tetrahedrane's large, unfavorable strain (141 kcal/mol)[61] leading to cage rupture. For example, the primary imaginary mode of $H^+@C_4H_4$ (T_d) leads to the cage-ruptured $C_4H_5^+$ C_s minimum shown in

(57) Koch, W.; Holthausen, M. C. *A Chemist's Guide to Density Functional Theory*; Wiley-VCH: Weinheim, 2000.
(58) Jimenez-Vazquez, H. A.; Tamariz, J.; Cross, R. J. *J. Phys. Chem. A* **2001**, *105*, 1315.
(59) Glendening, E. D.; Reed, A. E.; Carpenter, J. E.; Weinhold, F. *NBO*, version 3.1; University of Wisconsin: Madison, 1993.
(60) Frisch, M. J.; Trucks, G. W.; Schlegel, H. B.; Scuseria, G. E.; Robb, M. A.; Cheeseman, J. R.; Zakrzewski, V. G.; Montgomery, J. A. J.; Stratmann, R. E.; Burant, J. C.; Dapprich, S.; Millam, J. M.; Daniels, A. D.; Kudin, K. N.; Strain, M. C.; Farkas, O.; Tomasi, J.; Barone, V.; Cossi, M.; Cammi, R.; Mennucci, B.; Pomelli, C.; Adamo, C.; Clifford, S.; Ochterski, J.; Petersson, G. A.; Ayala, P. Y.; Cui, Q.; Morokuma, K.; Malick, D. K.; Rabuck, A. D.; Raghavachari, K.; Foresman, J. B.; Cioslowski, J.; Ortiz, J. V.; Stefanov, B. B.; Liu, G.; Liashenko, A.; Piskorz, P.; Komaromi, I.; Gomperts, R.; Martin, R. L.; Fox, D. J.; Keith, T.; Al-Laham, M. A.; Peng, C. Y.; Nanayakkara, A.; Gonzalez, C.; Challacombe, M.; Gill, P. M. W.; Johnson, B.; Chen, W.; Wong, M. W.; Andres, J. L.; Gonzalez, C.; Head-Gordon, M.; Replogle, E. S.; Pople, J. A. *Gaussian 98*, revision A.5; Gaussian, Inc.: Pittsburgh, PA, 1998.
(61) Wiberg, K. B.; Bader, R. F. W.; Lau, C. D. H. *J. Am. Chem. Soc.* **1987**, *109*, 1001.

Table 1. Distances between Cage Centers and the Closest Carbon Atom and C−C Bond Center (Å)[a]

	C_4H_4 (T_d)	C_8H_8 (O_h)	C_8H_{14} (D_{3h})	$C_{10}H_{16}$ (T_d)	$C_{12}H_{12}$ (T_d)	$C_{16}H_{16}$ (D_{4d})	$C_{20}H_{20}$ (I_h)
cage	0.906	1.360	1.299[b]	1.546	1.772	1.816[c]	2.180
face	0.302	0.785	0.726	0.771	0.927	1.410	1.732
bond	0.523	1.110	1.268[b]	1.478	1.601	1.639[c]	2.037
volume	0.143	1.368	2.039	3.229	4.104	4.403	8.452

[a] Cage faces are not useful because they are not often flat, and this makes the assignment of position and its implications arbitrary. [b] $C_{10}H_{16}$ bridgehead carbon and C−C bond. [c] Carbon and C−C bond in cage "equator".

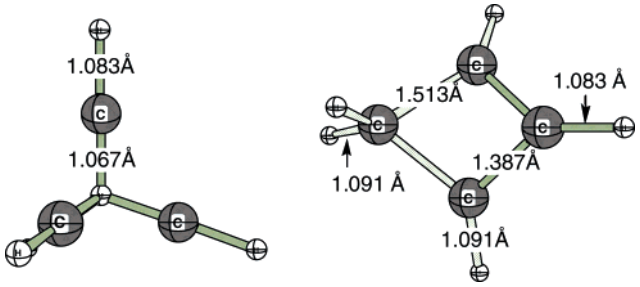

Figure 3. $H^+@C_4H_4$ (T_d) higher order stationary point structure (NImag = 5) and its C_s symmetric $C_4H_5^+$ cage-ruptured, isomeric minimum that is 331 kcal/mol more stable.

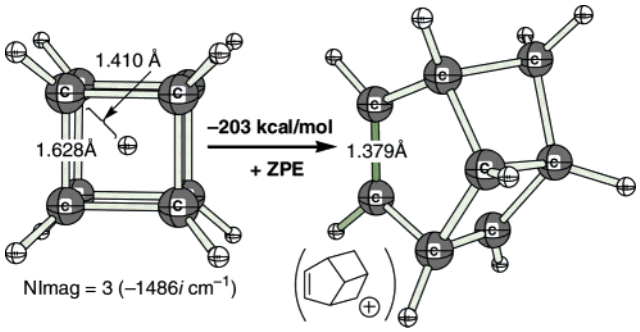

Figure 4. The $H^+@C_8H_8$ higher order stationary point structure and its $C_8H_9^+$ cage-ruptured, isomeric minima.

Figure 3, which is 331 kcal/mol lower in energy than its endohedral T_d isomer.

X@C$_8$H$_8$ (O_h). With the exception of $He@C_8H_8$, $Li^+@C_8H_8$, and $Be^{2+}@C_8H_8$, all other O_h cubane endohedral species are higher order stationary points leading to cage rupture. Like tetrahedrane, the dearth of endohedral complex minima is mainly due to cubane's small internal cavity (1.368 Å^3; Table 1) and highly unfavorable strain (∼159 kcal/mol).[61] Endohedral protonated cubane has three imaginary frequencies (triply degenerate 1486*i* cm^{-1}), and its cage-ruptured $C_8H_9^+$ isomer is 203 kcal/mol more stable (Figure 4). $H@C_8H_8$ also has three imaginary frequencies (triply degenerate 1222*i* cm^{-1}) which lead, as shown in Figure 5, to C_{4v} expulsion of the endohedral hydrogen via a cubane face. The dissociated H and C_8H_8 complex is 169 kcal/mol more stable than O_h $H@C_8H_8$, but 60 kcal/mol less stable than an alternative cage-ruptured C_s minima, with a hydrogen inserted into a C−C bond. The ruptured cubane metal, cation, and dication complexes fall into the C_{2v} (Li, Be^+, Na, Mg) and C_s (Be, Na, Mg, Na^+, Mg^+, Mg^{2+}) symmetric structural categories shown in Figure 6. They are much lower (>100 kcal/mol) in energy than their O_h endohedral higher order stationary point isomers. The NICS values at the C_{2v} and C_s complex ring centers (see Figure 7) are negative (diatropic) for

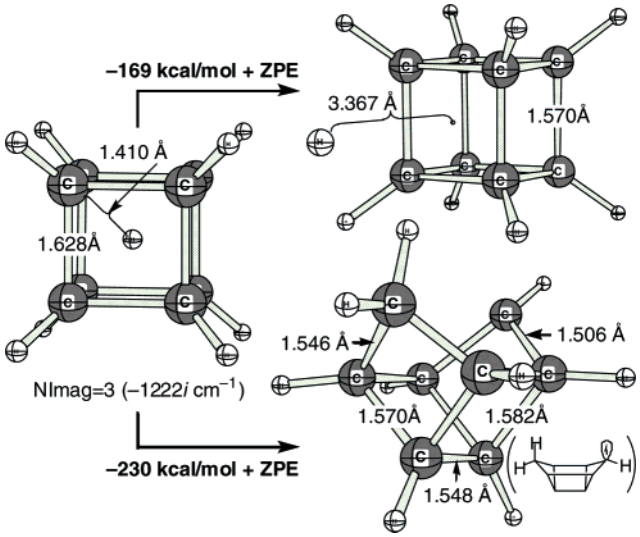

Figure 5. The $H@C_8H_8$ (O_h) higher order stationary point structure, which leads to a C_{4v} exohedral $H+C_8H_8$ minimum. A C_s cage-ruptured C_8H_9 structure also was located.

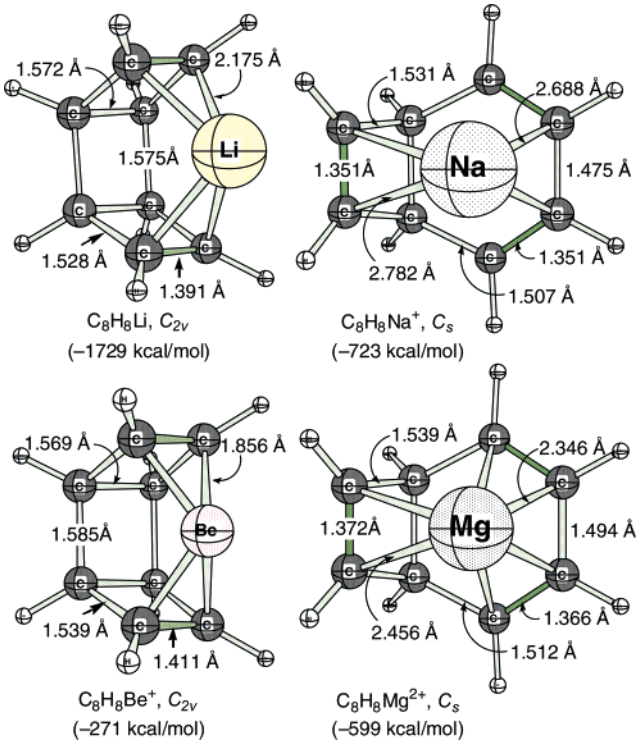

Figure 6. Examples of cage-ruptured cubane complexes and their energies relative to their endohedral complexes which are higher order stationary points.

three-membered rings (3MR) and positive (paratropic) for four-membered rings (4MR), as expected from calculations on the cyclopropane, cyclobutane, etc. parent molecules.[62]

$He@C_8H_8$, $Li^+@C_8H_8$, and $Be^{2+}@C_8H_8$ are O_h endohedral minima. In contrast to $Be^{2+}@C_8H_8$, which is ∼70 kcal/mol more stable than its isolated components, the $He@C_8H_8$ and $Li^+@C_8H_8$ inclusion energies shown in Table 2 are >200 kcal/mol endothermic. Furthermore, Li^+ and Be^{2+} have relatively large exothermic exohedral cubane binding energies, and all three endohedral complexes are >150 kcal/mol unfavorable relative

(62) Moran, D.; Manoharan, M.; Heine, T.; Schleyer, P. v. R. *Org. Lett.* **2003**, *5*, 23.

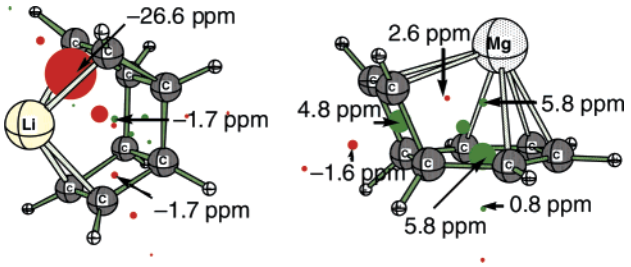

Figure 7. C_8H_8Li (C_{2v}; left) and $C_8H_8Mg^{2+}$ (C_s; right) nucleus independent chemical shifts (NICS).

Table 2. Symmetry-Optimized C_8H_8 (O_h), C_8H_{14} (D_{3d}), and $C_{10}H_{16}$ (T_d) Endohedral Complex Minima Inclusion, Binding, and Isomerization Energies and the Natural Charge on the Endohedral Species

	E_{inc} (kcal/mol)	E_{bind} (kcal/mol)	E_{isom} (kcal/mol)	charge X@
$He@C_8H_8$	332.3	0.1	−332.1	0.13
$Li^+@C_8H_8$	245.1	−26.6	−271.8	0.60
$Be^{2+}@C_8H_8$	−69.8	−222.0	−152.2	1.46
$He@C_8H_{14}$	214.2	0.1	−214.1	0.09
$Li@C_8H_{14}$	178.9	−0.1	−178.9	0.33
$Li^+@C_8H_{14}$	103.7	−26.3	−130.0	0.75
$Be^{2+}@C_8H_{14}$	−208.3	−230.0	−21.8	1.63
$H@C_{10}H_{16}$	101.2	−0.3	−101.5	0.23
$He@C_{10}H_{16}$	159.9	−0.2	−160.2	0.09
$Ne@C_{10}H_{16}$	364.5	−2.5	−367.0	0.12
$Li@C_{10}H_{16}$	144.9	−0.5	−145.4	0.25
$Li^+@C_{10}H_{16}$	60.0	−23.8	−83.8	0.72
$Na@C_{10}H_{16}$	359.1	−0.4	−359.5	0.15
$Na^+@C_{10}H_{16}$	284.7	−14.8	−299.5	0.76
$Be@C_{10}H_{16}$	225.2	−0.4	−225.6	1.51
$Be^+@C_{10}H_{16}$	57.2	−50.5	−107.7	1.58
$Be^{2+}@C_{10}H_{16}$	−235.5	−245.1	−9.5	1.69
$Mg^{2+}@C_{10}H_{16}$	62.7	−117.7	−180.4	1.75

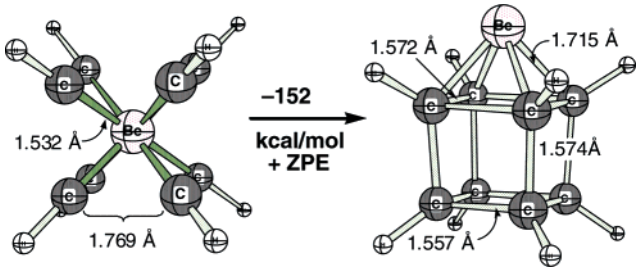

Figure 8. Endohedral and exohedral $C_8H_8Be^{2+}$ isomers and their relative energy, which is referred to in this paper as the "isomerization energy".

to their exohedral complexes (see Figure 8). Overall, cubane is an unsuitable host, irrespective of the size or charge of the guest.

$X@C_8H_{14}$ (D_{3h}). With the exception of He, Li, Li^+, and Be^{2+}, no other species are minima when encapsulated by D_{3h} symmetric C_8H_{14}. A proton at the cage center is a third-order stationary point (doubly degenerate 1260*i* cm^{-1} and 759*i* cm^{-1}), with the primary mode leading to C_{2v} H^+ expulsion (Figure 9) and the minor imaginary frequency corresponding to rapid (759*i* cm^{-1}) proton oscillation between the cage bridgehead carbons. A hydrogen atom at the cage center also is a third-order stationary point, corresponding to the hydrogen atom oscillation between bridgehead carbons (109*i* cm^{-1}) and C_{2v} hydrogen expulsion from the cage (doubly degenerate 104*i* cm^{-1}; same motion as shown in Figure 9 for H^+ expulsion). Following the mode of the first imaginary vibrational frequency of D_{3h}, $H@C_8H_{14}$ leads to a C_s cage-ruptured first-order stationary point

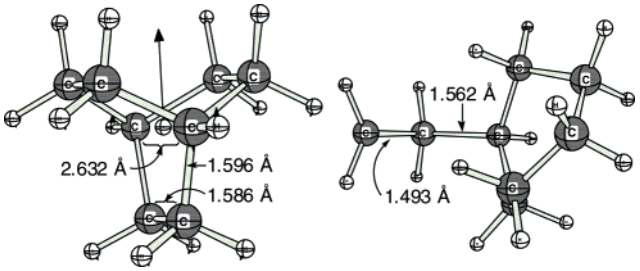

Figure 9. (Left) The $H^+@C_8H_{14}$ (D_{3h}) third-order stationary point and its first imaginary mode (1260*i* cm^{-1}) which corresponds to proton expulsion. (Right) Mode following the $H@C_8H_{14}$ (D_{3h}) first imaginary frequency (109*i* cm^{-1}) leads in two steps to a cage-ruptured C_1 minima, which is 127 kcal/mol more stable than its D_{3h} parent.

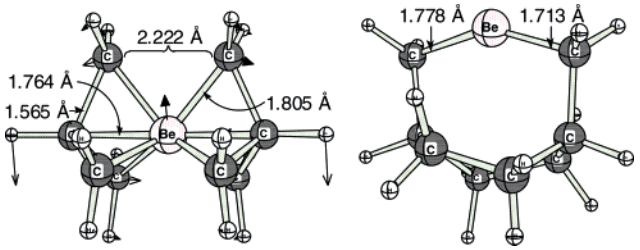

Figure 10. (Left) The first imaginary mode (1362*i* cm^{-1}) of the second-order stationary point structure $Be^+@C_8H_{14}$ (D_{3h}). (Right) Following the mode leads to the Be^+ inserting into a cage C−C bond cage; the C_1 structure shown is 99 kcal/mol more stable than its D_{3h} parent.

(134*i* cm^{-1}), which is 121 kcal/mol lower in energy than its D_{3h} isomer. The C_s C_8H_{14} imaginary mode corresponds to ring twisting and leads to a C_1 twist boat minimum with a hyperconjugatively stabilized ethenyl radical substituent (see Figure 9), which is an additional 5 kcal/mol more stable than its D_{3h} endohedral parent isomer. Mode following the first D_{3h} $H^+@C_8H_{14}$ imaginary frequency leads to an analogous cage-ruptured structure, 60 kcal/mol more stable than its D_{3h} parent isomer.

The remaining endohedral D_{3h} $X@C_8H_{14}$ complexes are at least second-order stationary points, with the cages split in half as shown for $Be^+@C_8H_{14}$ (doubly degenerate 1362*i* cm^{-1}) in Figure 10. In the case of D_{3h} $Ne@C_8H_{14}$, the 2.222 Å separation between cage halves shown in Figure 10 increases to 4.154 Å, and the limits of encapsulation are clearly demonstrated. Mode following and C_1 optimization for the beryllium and magnesium cation and dication systems lead to their insertion into non-bridgehead C−C bonds, as shown for $C_8H_{14}Be^+$ in Figure 10.

$X@C_{10}H_{16}$ (T_d). The moderately sized adamantane[47−49] molecule is possibly the most enigmatic host cage computed in this study, as the majority of adamantane endohedral complexes are minima (see Table 2). Species which are not T_d minima at the cage center include Ar (NImag = 9), Mg (NImag = 5), and Mg^+ (NImag = 3), as they are too large to fit inside the $C_{10}H_{16}$ host. Internally protonated adamantane also is a third-order stationary point (triply degenerate 1396*i* cm^{-1}), leading to proton attack of a nonbridgehead cage carbon and the formation of secondary carbocation minima 67 kcal/mol lower in energy than its endohedral parent (Figure 11). Placing an endohedral proton C_{3v} along a three-fold axis of symmetry and optimizing did not lead to proton expulsion via a cage face as expected, but located a second-order stationary point (doubly degenerate 1342*i* cm^{-1}) that also leads to proton attack on a nonbridgehead cage carbon.

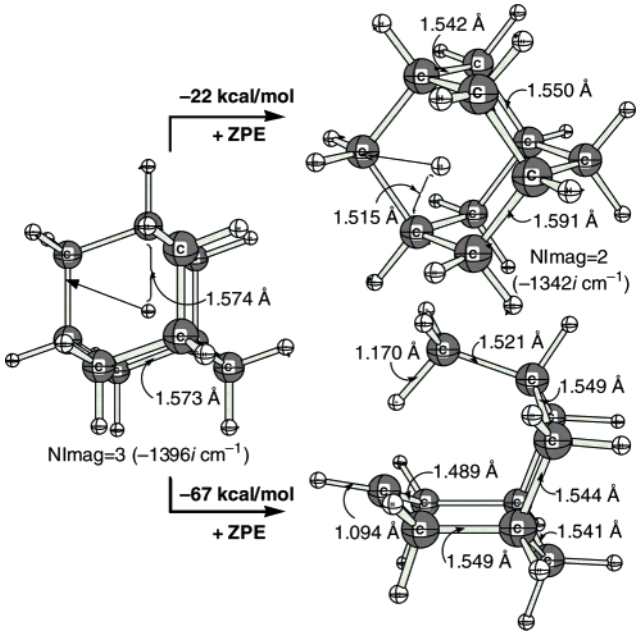

Figure 11. The $H^+@C_{10}H_{16}$ (T_d) third-order stationary point structure leading to a C_{3v} face localized second-order stationary point structure (top right) and C_s symmetric cage-ruptured $C_{10}H_{17}^+$ minima (bottom right).

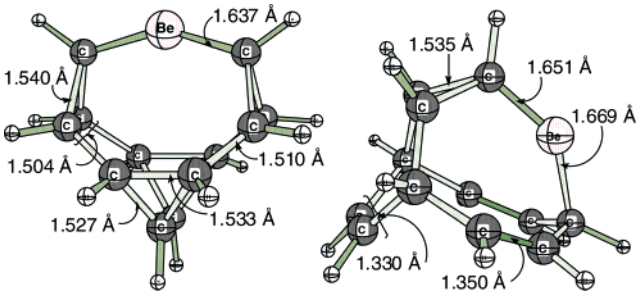

Figure 12. The $Be@C_{12}H_{12}$ (T_d) complex is a third-order stationary point. Mode following leads to the C_{2v} (left) and C_s (right) $C_{12}H_{12}Be$ complexes shown, which are 252 and 262 kcal/mol, respectively, more stable than their endohedral isomer.

$X@C_{12}H_{12}$ (T_d). Despite its increased internal cavity (Table 1), fewer endohedral species are minima at the $C_{12}H_{12}$ cage center as compared to adamantane (see Table 2). Species which are not T_d minima at the cage center include Ar (NImag = 5) and Be (NImag = 3), while Na, Mg, and Mg^+ T_d endohedral complex geometry optimizations failed to converge. An endohedral argon atom roughly exits the cage via an edge (i.e., no C−C bonds are broken) without barrier. In contrast, an endohedral Be inserts into a cage C−C bond, as shown in Figure 12, to form a C_{2v} symmetric complex favored by 252 kcal/mol. Relaxing symmetry constraints and reoptimizing the C_{2v} symmetric $C_{12}H_{12}Be$ structure lead to a C_s minimum, a further 10 kcal/mol (i.e., 262 kcal/mol total) more stable than the T_d third-order stationary point. NICS values at the C_{2v} and C_s $C_{12}H_{12}Be$ cage and ring centers (Figure 13) show the shielding effects due to the 3MRs,[62] with the later possessing an aromatic (−11.1 ppm) cage center.

As expected from the smaller host cage rearrangements (*vide supra*), internally protonated $C_{12}H_{12}$ is a third-order T_d stationary structure (triply degenerate 1467*i* cm^{-1}) corresponding to proton attack on a strained cyclopropane C−C bond (see Figure 14). With two double bond centers forming and the cation center localizing in a cyclopropenium moiety, the $C_{12}H_{13}^+$ cage

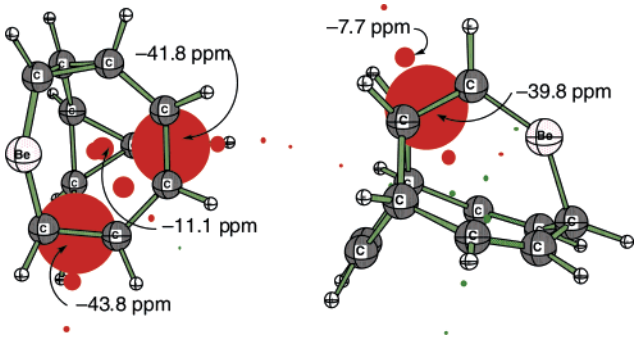

Figure 13. C_{2v} (left) and C_s (right) $C_{12}H_{12}Be$ NICS.

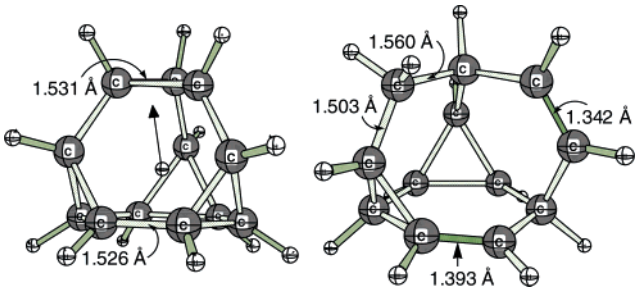

Figure 14. (Left) $H^+@C_{12}H_{12}$ (T_d) is a third stationary structure (triply degenerate 1467*i* cm^{-1}) corresponding to proton attack of the strained cyclopropane C−C bond. (Right) Mode following leads to a C_1 cage-ruptured structure 149 kcal/mol lower in energy.

ruptures, and the new structure is 149 kcal/mol more stable than its T_d endohedral isomer.

$C_{12}H_{12}$ offers three (3MRF)- and six (6MRF)-membered ring cage faces for coordination with exohedral species. He and Ne weakly prefer 3MRF coordination by 0.1 and 0.6 kcal/mol, respectively. Hydrogen and lithium atoms have a weak (3.3 and 3.8 kcal/mol, respectively) preference for the 6MRF, while charged species strongly favor (>20 kcal/mol) the larger cage face; Li^+, Na^+, Be^{2+}, and Mg^{2+} favor the 6MRF by 28, 19, 88, and 61 kcal/mol, respectively.

$X@C_{16}H_{16}$ (D_{4d}). The majority of endohedral $X@C_{16}H_{16}$ species have D_{4d} minima. The expected (*vide supra*) exceptions are mostly higher order saddle points leading to $C_{16}H_{16}$ cage rupture: H^+ (NImag = 2, cage rupture); Be (NImag = 3, cage rupture); Mg^+ (NImag = 2, cage rupture); and Mg (geometry optimization failed to converge). Unexpectedly, neither Be^+ (2604*i* cm^{-1} and doubly degenerate 532*i* cm^{-1}) nor Be^{2+} (257*i* cm^{-1}) are minima at the cage center; however, following their primary imaginary modes leads to the C_{4v} face localized minima shown in Figure 15. This is the same behavior as that for $Be^+@C_{20}H_{20}$ and $Be^{2+}@C_{20}H_{20}$, which in preference to I_h cage-centered structures are C_{5v} symmetrically localized against an interior dodecahedrane face.[11] The tendency for small species to face localize was tested by placing an endohedral helium atom against a four-membered ring cage face, in the same geometry as was observed for C_{4v} $Be^{2+}@C_{16}H_{16}$. However, optimization results in movement of the helium atom back to the cage center; that is, an approximately D_{4d} structure develops. $Be@C_{16}H_{16}$ is a D_{4d} minimum, although it spontaneously dissociates into a (cyclobutadiene)Be(*nido*-$C_{12}H_{12}$) upon C_{4v} geometry optimization (see Supporting Information).

Endohedrally protonated $C_{16}H_{16}$ undergoes a variety of interesting rearrangements, as shown in Figure 16. At the cage center (D_{4d}), the proton encapsulating complex is a second-order

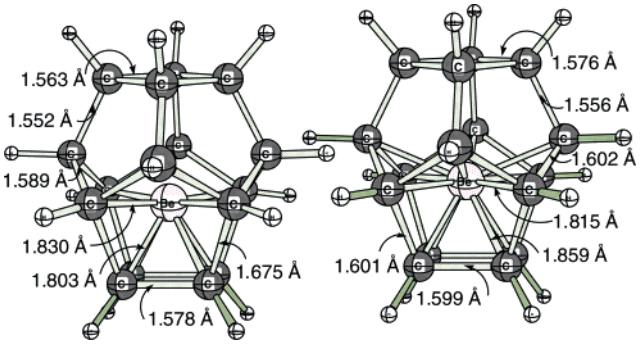

Figure 15. Face localized $Be^{+}@C_{16}H_{16}$ (left) and $Be^{2+}@C_{16}H_{16}$ (right) C_{4v} symmetric minima. They are 10 and 2 kcal/mol, respectively, more stable than their D_{4d} cage-centered isomers.

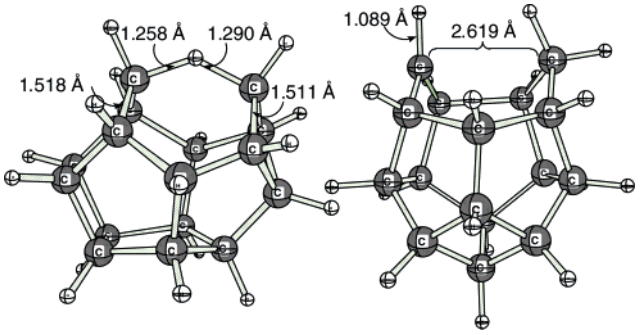

Figure 16. C_s (left) and C_1 (right) $C_{16}H_{17}^{+}$ minima. They are 90 and 109 kcal/mol, respectively, more stable than their D_{4d} cage-centered $H^{+}@C_{16}H_{16}$ isomer.

stationary point (doubly degenerate 1612*i* cm^{-1}) with the imaginary modes corresponding to proton attack of an "equatorial" C−H carbon. Mode following leads to a C_s minimum with a structure very similar to that of protonated dodecahedrane, $C_{20}H_{21}^{+}$ (C_{2v}), in which the proton symmetrically bridges two carbon atoms.[17] With an endohedral proton against a four-membered ring cage face, in the same geometry as observed for C_{4v} $Be^{2+}@C_{16}H_{16}$, optimization results in barrierless proton migration through the face to the cage exterior, that is, exohedral coordination. An endohedral hydrogen atom placed against a four-membered ring cage face, however, simply moves back to the cage center, reproducing the D_{4d} symmetric minimum structure. The exohedral $C_{16}H_{16}$ bound proton structure also is a second-order stationary point (doubly degenerate 916*i* cm^{-1}); mode following leads to a C_1, cage-ruptured minimum 109 kcal/mol more stable than its endohedral D_{4d} cage-centered $H^{+}@C_{16}H_{16}$ isomer.

$C_{16}H_{16}$ also has two different kinds of exterior faces, incorporating four (4MRF)- and five (5MRF)-membered rings, to which exohedral species can coordinate. The small species H and He weakly prefer 4MRF coordination, while neon, lithium, and sodium atoms have a weak preference for the 5MRF. Charged species favor the larger cage face with Li^{+}, Na^{+}, Be^{+}, Be^{2+}, and Mg^{2+} 5MRF binding energies of −3.8, −2.6, −6.6, −24.5, and −12.0 kcal/mol, respectively.

Complex Stabilities. The theoretical inclusion, binding, and isomerization energies are summarized in Tables 2 and 3. The inclusion energies are related to the size and charge of the endohedral species and the volume of host cavity. The latter point is demonstrated in Figure 17, which shows He and Li^{+} inclusion energies plotted as a function of cage volume (the volume is calculated using the distance from the cage center to the midpoint of the nearest C−C bond). For both neutral (closed shell) helium and lithium cation, the inclusion energies smoothly decrease as the cage volume increases from 1.4 (C_8H_8) to 8.5 $Å^3$ ($C_{20}H_{20}$). There is no evidence of cage strain effects, that is, cages with different intrinsic strain energies having particularly poor inclusion energies, although qualitatively cage strain energies are indicative of the maximum species size a cage can encapsulate (*vide infra*). For example, $C_{12}H_{12}$ has a large strain energy (101 kcal/mol),[50] and yet there is a linear relationship ($R = 0.997$) between its E_{inc} and those for $C_{10}H_{16}$, which is only strained by 7 kcal/mol[50] (see Figure 18).

Table 3. Symmetry-Optimized $C_{12}H_{12}$ (T_d) and $C_{16}H_{16}$ (D_{4d}) Endohedral Complex Minima Inclusion, Binding, and Isomerization Energies and the Natural Charge on the Endohedral Species

	E_{inc} (kcal/mol)	E_{bind} (kcal/mol)	E_{isom} (kcal/mol)	charge X@
$H@C_{12}H_{12}$	86.4	−3.5	−89.9	0.15
$He@C_{12}H_{12}$	119.3	−0.1	−119.4	0.07
$Ne@C_{12}H_{12}$	287.0	−2.3	−289.3	0.12
$Li@C_{12}H_{12}$	143.4	−3.6	−147.0	0.21
$Li^{+}@C_{12}H_{12}$	50.2	−47.7	−97.8	0.73
$Na^{+}@C_{12}H_{12}$	237.2	−31.0	−268.2	0.80
$Be^{2+}@C_{12}H_{12}$	−181.2	−290.0	−108.8	1.75
$Mg^{2+}@C_{12}H_{12}$	45.0	−154.6	−199.7	1.77
$H@C_{16}H_{16}$	65.2	0.0	−65.2	0.13
$He@C_{16}H_{16}$	90.3	−0.1	−88.2	0.06
$Ne@C_{16}H_{16}$	207.3	−4.7	−212.0	0.12
$Ar@C_{16}H_{16}$	548.0	−0.9	−546.1	0.46
$Li@C_{16}H_{16}$	105.8	−0.8	−106.5	0.28
$Li^{+}@C_{16}H_{16}$	13.3	−35.0	−48.3	0.70
$Na@C_{16}H_{16}$	237.9	0.0	−237.9	0.16
$Na^{+}@C_{16}H_{16}$	157.5	−21.5	−179.1	0.75
$Be^{+}@C_{16}H_{16}$[a]	31.8	−59.6	−91.4	1.59
$Be^{2+}@C_{16}H_{16}$[a]	−239.2	−257.1	−17.8	1.73
$Mg^{2+}@C_{16}H_{16}$	−37.7	−130.6	−92.9	1.65

[a] C_{4v} minimum.

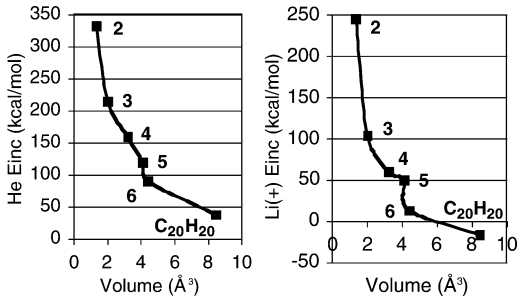

Figure 17. Relationship between cage volume and helium and lithium inclusion energies. The different cages are distinguished by the labels 2−6 (see Figure 1). Cage volumes were calculated using the distance from cage centers to the midpoints of the closest adjacent C−C bonds.

Dodecahedrane encapsulation of hydrogen (E_{inc} = 36 kcal/mol)[17] and helium (E_{inc} = 38 kcal/mol)[17] is much preferred to encapsulation by $C_{16}H_{16}$ or smaller cages. The $C_{10}H_{16}$ endohedral complex inclusion energies increase in the series (Figure 19): Be^{2+} (E_{inc} = −236 kcal/mol) > Li^{+} (E_{inc} = 60 kcal/mol) > H (E_{inc} = 101 kcal/mol) > Li (E_{inc} = 145 kcal/mol) > He (E_{inc} = 160 kcal/mol). The surprising preference for lithium metal encapsulation as compared to helium is explained by its significant (+0.25 electrons) positive partial charge. Isomerization energies are always exothermic, and exohedral coordination is preferred to endohedral encapsulation without exception. Of note are $Be^{2+}@C_8H_{14}$ (E_{isom} = −22 kcal/mol), $Be^{2+}@C_{10}H_{16}$ (E_{isom} = −10 kcal/mol), $Li^{+}@C_{16}H_{16}$ (E_{isom} = −45 kcal/mol),

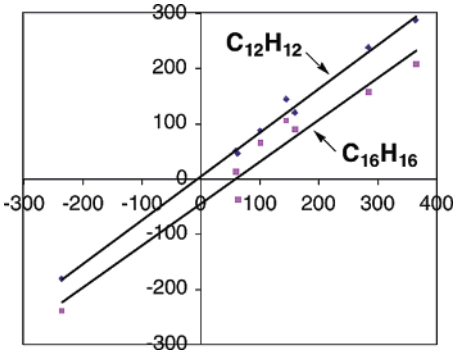

Figure 18. $C_{12}H_{12}$ and $C_{16}H_{16}$ inclusion energies (kcal/mol) plotted versus the $C_{10}H_{16}$ inclusion energies (kcal/mol) summarized in Tables 2 and 3. The highly correlated ($r \geq 0.98$) lines of best fit highlight the lack of relationship between intrinsic cage strain and endohedral complex inclusion energy.

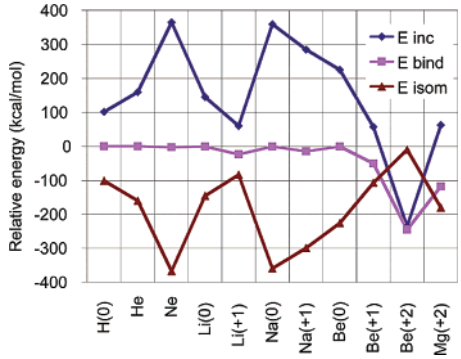

Figure 19. Adamantane inclusion, binding, and isomerization energy trends.

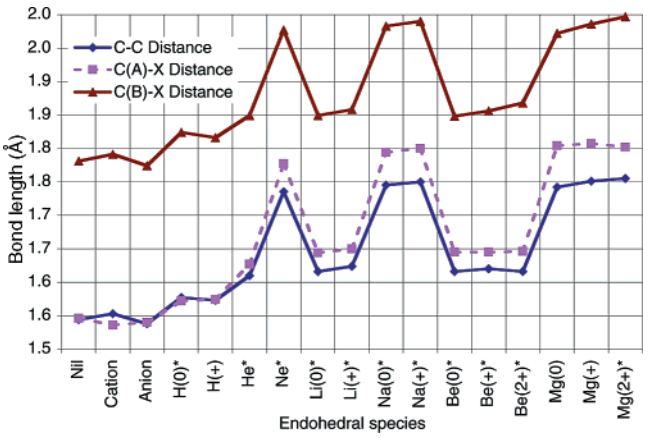

Figure 20. Endohedral T_d $C_{10}H_{16}$ derivative bond length trends.

and $Be^{2+}@C_{16}H_{16}$ ($E_{isom} = -18$ kcal/mol), which are stabilized by the combination of strong charge polarization stabilization and the relatively small endohedral species radii (Be^{2+}, after all, is the smallest possible metal cation, followed by Li^+). $Be^{2+}@C_{20}H_{20}$ (C_{5v}) also has an exothermic isomerization energy ($E_{isom} = -17$ kcal/mol);[11] although the dodecahedrane complex has a large inclusion energy (−236 kcal/mol), Be^{2+} binds the $C_{20}H_{20}$ cage exterior more tightly, and hence its isomerization energy is unfavorable.

Optimized Geometries. $X@C_{10}H_{16}$-, $X@C_{12}H_{12}$-, and $X@C_{16}H_{16}$-optimized C−C bond lengths are summarized graphically in Figures 20−22, respectively. Reviewing these plots, it is obvious that cage C−C bond lengths are shorter when hosting a neutral metal as compared to its corresponding cation/dication. For example, the C−C bond length of $Li@C_{10}H_{16}$ is

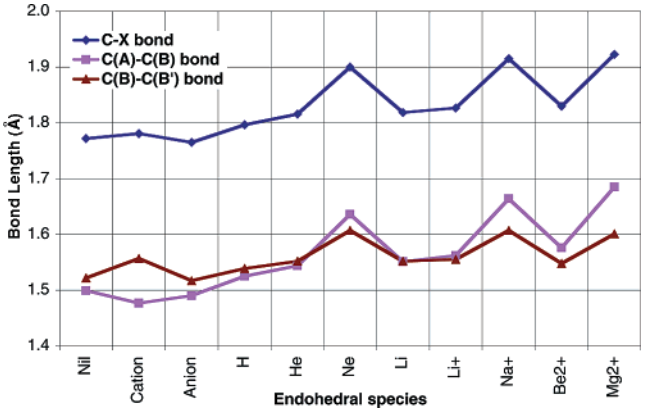

Figure 21. Endohedral T_d $C_{12}H_{12}$ complex C−C and CX bond lengths.

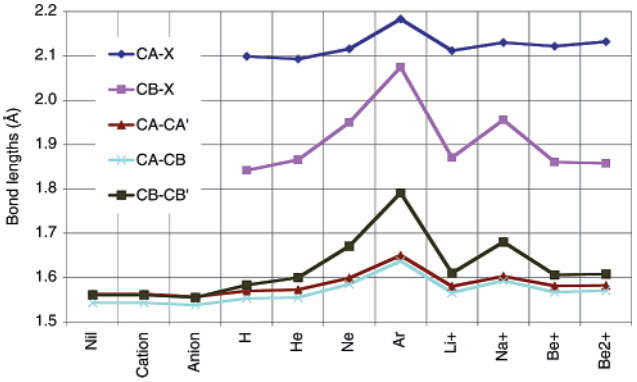

Figure 22. Endohedral $C_{16}H_{16}$ complex C−C and CX bond lengths.

1.616 Å, while that of $Li^+@C_{10}H_{16}$ is 1.624 Å. Previously,[11] we observed analogous behavior for the optimized geometries of $X@C_{20}H_{20}$ endohedral complexes, which was caused by donation of electron density from the encapsulated metal atom into their C−C bonding and C−H antibonding endohedral complex highest occupied molecular orbitals (HOMOs). Note that these HOMOs had structures closely resembling the lowest unoccupied molecular orbital (LUMO) of dodecahedrane. Surveying Tables 2 and 3, it is clear that, independent of the cage, encapsulated metals (Li, Na, Be) are significantly ionized through charge donation to the host. Hence the same molecular orbital argument explains the trend of $C_{10}H_{16}$, $C_{12}H_{12}$, and $C_{16}H_{16}$ cages becoming more compact upon metal encapsulation, as all three cages have C−C bonding and C−H antibonding LUMOs (see Figure 23). The optimized geometries of cage-encapsulated noble gas atoms are more straightforward and increase on going from He to Ne, as expected due to their increasing atomic radii down the periodic table.

When comparing $C_{10}H_{16}$, $C_{12}H_{12}$, and $C_{16}H_{16}$, there is a qualitative relationship between cage strain, internal volume, and potential to form an endohedral complex potential energy minima. This is best illustrated using examples and by focusing on adamantane, which is strained by a mere 6.6 kcal/mol[63] and has a moderate endohedral volume of ~3.2 Å^3. T_d symmetric $C_{10}H_{16}$ is able to form endohedral complexes with large metal species such as Na and Be, while strained (101 kcal/mol)[50] $C_{12}H_{12}$, in contrast, which has a larger internal cavity (~4.1 Å^3), ruptures when species larger than Ne and Li are placed inside, with large associated enthalpic gains. $C_{16}H_{16}$, the largest

(63) Schleyer, P. v. R.; Williams, J. E.; Blanchard, K. R. *J. Am. Chem. Soc.* **1970**, *92*, 2377.

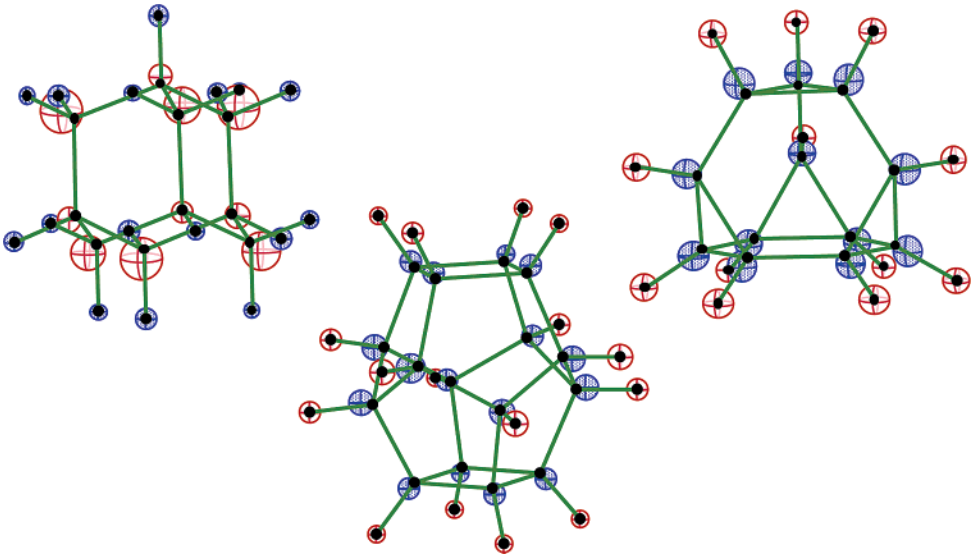

Figure 23. T_d $C_{10}H_{16}$ (left; A_1), T_d $C_{12}H_{12}$ (right; A_1), and D_{4d} $C_{16}H_{16}$ (center; B_2) lowest unoccupied molecular orbitals (LUMOs). Note that they are C−C bonding and C−H antibonding.

(∼4.4 Å^3) cage computed herein, encapsulates large species up to and including Ar, reflecting its relatively generous host cavity.

Excluding highly reactive proton and hydrogen moieties, which tend to destroy their hosts from the inside out, the situation for the smaller cages C_4H_4, C_8H_8, and C_8H_{14} is more straightforward. Tetrahedrane is highly strained (141 kcal/mol)[61] and has a relatively small internal volume (∼0.2 Å^3); hence all encapsulation ruptures the cage due to either mechanical effects or polarization of the bent[61] bonds. Cubane also is highly strained (159 kcal/mol);[61] however, it has sufficient volume (∼1.2 Å^3) to encapsulate very small species He, Li^+, and Be^{2+}. In contrast with C_4H_4 and C_8H_8, bicyclo[2.2.2]octane is strained by a mere 11 kcal/mol[61] and has a volume of ∼2.0 Å^3. It is able to encapsulate Li in addition to He, Li^+, and Be^{2+} and further exemplifies the encapsulation size effect highlighted by adamantane. Bicyclo[2.2.2]octane also illustrates that cage structure affects endohedral complex formation, as its non-bridgehead C−C bonds are exposed to endohedral electrophilic attack (see Figure 10 for examples of what happens) and the relatively large "windows" into the C_8H_{14} interior allow species to migrate out of the endohedral space (*vide supra*).

The proton affinities of the ruptured cages are as follows: 331 kcal/mol (C_4H_4); 230 kcal/mol (C_8H_8); 60 kcal/mol (C_8H_{14}); 67 kcal/mol ($C_{10}H_{16}$); 149 kcal/mol ($C_{12}H_{12}$); and 90 kcal/mol ($C_{16}H_{16}$). For comparison, the proton affinity (PA) of protonated dodecahedrane, $C_{20}H_{21}^+$ (C_{2v}), in which the proton bridges two carbon atoms symmetrically, is 185 kcal/mol;[17] protonated ethane also has a proton-bridged C−C bond, but with a lower PA (143 kcal/mol).[64] The difference in PA between $C_{20}H_{20}$ and C_2H_6 is due to dodecahedrane's superior ability to disperse the resulting positive charge. In addition to size effects, there also is an important contribution from strain to C_4H_4−$C_{16}H_{16}$ PA trends.

Ionization Potentials. Adiabatic ionization potentials (IP) for Li, Na, Be, and Be^+ endohedral complexes are summarized in Table 4. The IPs of encapsulated species are reduced considerably relative to the free metal. This is consistent with our previous[11] results where Li, Na, Be, and Mg X@$C_{20}H_{20}$ first ionization potentials ranging from 2.7 (62 kcal/mol) to 3.4 eV (86 kcal/mol) were computed. Boldyrev and co-workers[65−67] defined species with first ionization potentials less than the Cs atom (3.9 eV; 90 kcal/mol) as "superalkalis", and that label is equally applicable to the metals in Table 4.

Table 4. Adiabatic Ionization Potentials for Free and Cage Encapsulated Metals (eV)

X	exp.[a]	free	C_8H_{14}	$C_{10}H_{16}$	$C_{12}H_{12}$	$C_{16}H_{16}$
$Li \rightarrow Li^+ + e^-$	5.39	5.61	2.23	1.83	1.32	1.44
$Na \rightarrow Na^+ + e^-$	5.14	5.42		2.11		1.85
$Be \rightarrow Be^+ + e^-$	9.32	9.11		1.45		
$Be^+ \rightarrow Be^{2+} + e^-$		18.59		5.48		6.83

[a] NIST Physics Laboratory − Physical Reference Data (www.nist.gov/chemistry).

Comparison of the IP in Table 4 reveals obvious size effects. For example, the lithium first ionization potentials go down in the series: C_8H_{14} (2.2 eV) > $C_{10}H_{16}$ (1.8 eV) > $C_{12}H_{12}$ (1.3 eV) ≈ $C_{16}H_{16}$ (1.4 eV). This trend is explicable in terms of molecular orbital arguments, as C_8H_{14} has less orbitals than $C_{16}H_{16}$, charge-transfer stabilization of its C−C LUMO will be greater, and hence an endohedral metal atom is more stable inside the larger cage. Sodium also has a higher IP when $C_{10}H_{16}$ (2.1 eV) is encapsulated as compared to $C_{16}H_{16}$ (1.9 eV).

Conclusions

As an encapsulating hydrocarbon framework, tetrahedrane has neither practical nor theoretical utility as the highly strained cage always ruptures. The next largest systems computed, C_8H_8 (O_h) and C_8H_{14} (D_{3h}), encapsulated He, Li^+, and Be^{2+}; however, their relatively small internal cavities produce highly unfavorable endohedral inclusion energies or endo → exo isomerization energies. For example, Li^+@C_8H_{14} (D_{3h}) E_{inc} = 103.7 kcal/mol and E_{isom} = −130.0 kcal/mol. Cubane and bicyclo[2.2.2]-octane, therefore, do not offer much promise as encapsulating

(64) Carneiro, J. W. M.; Schleyer, P. v. R.; Saunders, M.; Remington, R. B.; Schaefer, H. F.; Rauk, A.; Sorensen, T. S. *J. Am. Chem. Soc.* **1994**, *116*, 3483.
(65) Gutsev, G. L.; Boldyrev, A. I. *Adv. Chem. Phys.* **1985**, *51*, 169.
(66) Gutsev, G. L.; Boldyrev, A. I. *Chem. Phys. Lett.* **1982**, *92*, 262.
(67) Rehm, E.; Boldyrev, A. I.; Schleyer, P. v. R. *Inorg. Chem.* **1992**, *31*, 4834.

hosts either. Endohedrally protonated and hydrogenated cages undergo a myriad of structural rearrangements leading to cage-ruptured minima that are significantly lower (>100 kcal/mol) in energy than their cage-centered endohedral complex isomers, and they are not particularly viable synthetic targets.

The larger endohedral minima include: T_d X@$C_{12}H_{12}$ (X = H, He, Ne, Li, Li^+, Na^+, Be^{2+}, and Mg^{2+}); T_d X@$C_{10}H_{16}$ and D_{4d} X@$C_{16}H_{16}$ (X = H, He, Ne, Li, Li^+, Na, Na^+, and Mg^{2+}); cage-centered $Be^{0,+,2+}$@$C_{10}H_{16}$ (T_d) and Ar@$C_{16}H_{16}$ (D_{4d}); and face localized $Be^{+,2+}$@$C_{16}H_{16}$ (C_{4v}). Endohedral hydrogen and noble gas atoms (He, Ne, and Ar) stretch the cages roughly in proportion to their atomic radii, expanding, for example, the X@$C_{10}H_{16}$ (T_d) C−C bond lengths from 1.577 (H@$C_{10}H_{16}$) to 1.735 Å (Ne@$C_{10}H_{16}$). However, the trend is somewhat different, and the cages are slightly more compact when encapsulating metal atoms as compared to their corresponding cations or dications. For example, adamantane C−C bond lengths increase from 1.616 (Li@$C_{10}H_{16}$) to 1.624 Å (Li^+@$C_{10}H_{16}$). This is due to donation of electron density from encapsulated metal atoms into the C−C bonding and C−H antibonding endohedral complex HOMOs, which have structures closely resembling the LUMOs of their hosts.

X@$C_{10}H_{16}$, X@$C_{12}H_{12}$, and X@$C_{16}H_{16}$ inclusion energies are most favorable (i.e., <50 kcal/mol) for small, charged Li^+ and Be^{2+} species. The ZPE corrected inclusion energies of Be^{2+}@$C_{10}H_{16}$ (T_d; −235.5 kcal/mol), Li^+@$C_{12}H_{12}$ (T_d; 50.2 kcal/mol), Be^{2+}@$C_{12}H_{12}$ (T_d; −181.2 kcal/mol), Mg^{2+}@$C_{12}H_{12}$ (T_d; −45.0 kcal/mol), Li^+@$C_{16}H_{16}$ (D_{4d}; 13.3 kcal/mol), Be^+@$C_{16}H_{16}$ (C_{4v}; 31.8 kcal/mol), Be^{2+}@$C_{16}H_{16}$ (D_{4d}; −239.2 kcal/mol), and Mg^{2+}@$C_{16}H_{16}$ (D_{4d}; −37.7 kcal/mol) are exothermic or approaching thermoneutral as compared to their isolated components, due to polarization stabilization of these charged complexes. However, all of the endohedral complexes are higher in energy than their corresponding exohedral isomers; that is, exohedral binding is favored over endohedral encapsulation.

Although the prospects for preparing small (<$C_{20}H_{20}$) endohedral hydrocarbon cage complexes are poor, the complexes are not prohibitively unstable as compared to the experimentally known He@$C_{20}H_{20}$ endohedral complex (E_{inc} = 38.0 kcal/mol and E_{isom} = −35.4 kcal/mol). We conclude that the recipe for a viable endohedral cage complex is low parent cage strain energy, large cage internal cavity volume, and a small, highly charged guest species.

Acknowledgment. Support of this work by the University of Georgia and the U.S. National Science Foundation (Grant CHE-0209857) is gratefully acknowledged. We thank Dr. Eluvathingal Jemmis (University of Hyderabad, India) and Dr. Bruce King (University of Georgia) for fruitful discussions.

Supporting Information Available: Absolute energies, zero-point vibrational energies, and optimized endohedral bond lengths and HOMO/LUMO gaps (PDF). This material is available free of charge via the Internet at http://pubs.acs.org.

JA0345470